Sympathetic Cooling of $^{139}BaH^+$ Using Laser-Cooled $^{138}Ba^+$ in Linear RF Traps

Nikita Poljakov

Introduction

Simultaneous precision measurements on both hydrogen and antihydrogen allow to study the matter-antimatter asymmetry while avoiding systematic errors. Examples of such experiments include gravitational tests[1, 2] and spectroscopy[3, 4, 5, 6].

In ALPHA the first ingredient antihydrogen, is obtained using collisions of high-energy protons from the Large Hadron Collider with a fixed iridium target[7]. This project focused on obtaining and trapping the second ingredient, hydrogen, from barium monohydride and cooling it to sub-mK temperatures. The lower the temperature, the higher the precision of the measurement.

We consider obtaining hydrogen as follows. First, $^{138}Ba^+$ and $^{139}BaH^+$ ions are laser ablated from the surface of the barium hydride salt target. Subsequently, these ions can be trapped in a linear radio-frequency (RF) trap. Once the charged ions are hung in electric fields, Ba^+ ions can be laser cooled using the 493 nm transition line. Cool Ba^+ ions then interact with hotter BaH^+ ions via Coulomb forces and the ion ensemble cools down as a whole, which is known as the sympathetic cooling[8]. Finally, hydrogen is photodissociated from the BaH^+ ions using a ~ 415 nm laser beam and becomes ~ 139 times colder than the ion before photodissociation[9].

The absence of nuclear spin in $^{138}Ba^+$ means that there is no hyperfine splitting in electron energy levels. Therefore, these ions are easier to laser cool than e.g. $^{137}Ba^+$ and $^{9}Be^+$.

The use of a linear RF trap has at least two advantages: 1) particles can be introduced or extracted from multiple angles; the lasers can be introduced along at least three different axes; 2) the absence of significant magnetic fields does not cause splitting of otherwise degenerate energy levels which simplifies laser cooling.

In this report we present the results of simulating sympathetic cooling of BaH^+ ions using laser-cooled Ba^+ ions in linear RF quadrupole and octupole traps. We show that it is possible to bring ions to a crystal state and obtain $0.1-100$ mK hydrogen. The simulation relied on the ideas used in other RF trap molecular dynamics simulations[10, 11].

Theory

Linear Quadrupole Trap

A linear RF trap is a device that uses time-varying electric potentials applied on cylindrical rods to trap charged particles. We consider a quadrupole with dimensions and voltages shown in FIG 1 with cylindrical endcaps. As we will later see, this configuration yields a simple ion trajectory stability analysis[12].

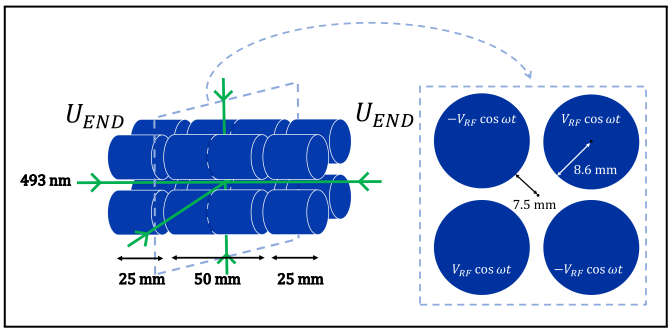

Figure 1. A linear quadrupole RF trap with cylindrical endcaps and its cross-section. A RF-voltage source with amplitude V_{RF} and angular frequency ω is connected to all rods to trap charged particles radially. Additionally, a DC voltage source U_{END} is applied to the endcaps to trap charged particles axially. The distance from the axis to the rod surface is $r_0 = 7.5$ mm and the radius of the rods is 1.1468 times larger. The green arrows indicate the directions of laser cooling beams with a wavelength 493 nm.

Similar to the original hyperbolic quadrupole trap proposed by Wolfgang Paul[13], it can be shown that the charges in our trap obey the Mathieu equations,

$$\ddot{x} = (a + 2q\cos 2\tau)x, \tag{1}$$
$$\ddot{y} = (a - 2q\cos 2\tau)y, \tag{2}$$

where $a = \frac{4e\alpha U_{END}}{m\omega r_0^2}$ and $q = \frac{2eV_{RF}}{m\omega r_0^2}$ are the dimensionless Mathieu parameters, and the derivatives are taken with respect to the dimensionless time $\tau = \frac{1}{2}\omega t$.

Only for certain values of a and q can the ion's trajectory remain bounded. Notice the parameter α in the

definition of a. It depends on the geometry of the trap and is due to the assumption that the endcap potential acts on the charged particle radially the same way as middle rods with the potential αU_{end} would and hence can take values in the interval $[-1,0]$.

For sufficiently high values of ω an adiabatic approximation can be made[14]. In particular, the radial motion of particles $r(t)$ can be decoupled into micromotion $\delta(t)$ and secular motion $\Delta(t)$: $r(t) = \delta(t) + \Delta(t)$. The former oscillates rapidly with the AC frequency ω of the electrodes with small amplitudes while the latter oscillates slowly with larger amplitudes. Averaging over the micromotion, a harmonic pseudo-potential can be obtained,

$$V(r,z) = \frac{m\omega^2(a+\frac{q^2}{2})}{8} r^2 - \frac{m\omega^2 a}{4} z^2. \tag{3}$$

The secular motion is due to the force generated by the pseudopotential. Furthermore, it can be shown that the amplitude in micromotion oscillations is proportional to the radial distance from the main axis of the trap, $\delta(t) = \frac{q\Delta(t)}{2}\cos 2\tau$ [14]. Therefore, ions farther away from the trap axis tend to be hotter than the ones closer to the axis.

Linear Octupole Trap

A multipole trap has a flatter potential than a quadrupole trap, and as the number of poles is increased, its potential approximates a box potential. A complex configuration is paid off by the vanishing micromotion in flatter potential regions. Therefore, multipole traps allow to cool ions to lower temperatures than quadrupole traps.

For the octupole trap, we consider a configuration similar to the quadrupole one but with the reduced radius to 2.5 mm as suggested by [15]. The dimensions and voltages are illustrated in FIG 2.

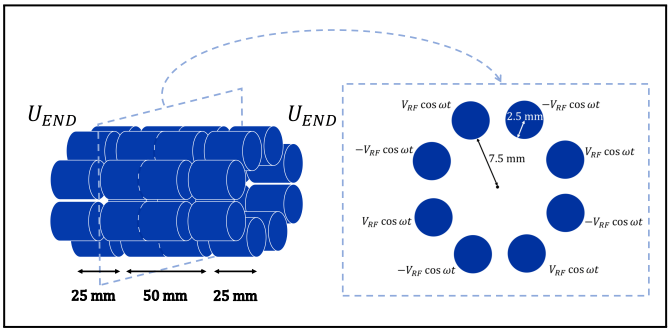

Figure 2. A linear octupole RF trap with cylindrical endcaps and its cross-section. The RF voltages of neighbouring rods are in opposite phases.

Unfortunately, the stability of ion trajectories in multipole traps depends on the initial position of the ion and and hence cannot be described using a two-dimensional stability parameter space like for the quadrupole trap. However, stability can be described locally using the adiabadicity parameter $\eta = \frac{2e\vec{\nabla}\cdot\vec{E}}{m\omega^2}$, where the ion trajectory is stable for $\eta < 0.3$ [16].

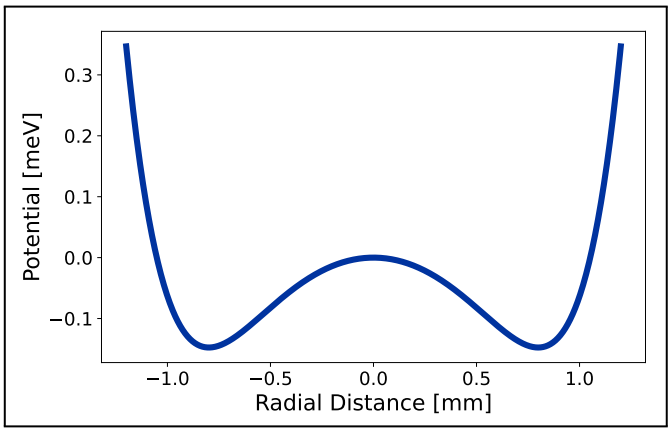

Figure 3. The octupole radial potential is a sum of the non-harmonic RF pseudopotential and a defocussing harmonic endcap potential. The potential minimum is at $r \approx 0.8$ mm.

The octupole RF voltage accelerates the charged particles the following way[17],

$$\ddot{x} = \frac{2ex^3}{mr_0^4}\left(1 - \frac{3y^2}{x^2}\right) V_{RF}\cos\omega t, \tag{4}$$

$$\ddot{y} = \frac{2ey^3}{mr_0^4}\left(1 - \frac{3x^2}{y^2}\right) V_{RF}\cos\omega t. \tag{5}$$

Similar to quadrupoles, an octupole pseudopotential can be derived[15]. As seen in the FIG 3, the RF voltage of the octupole produces a sixth-order radial potential while the DC voltage applied to the endcaps adds a quadratic radial defocussing,

$$V(r,z) = \frac{e^2 V_{RF}}{m\omega^2 r_0^2}\left(\frac{r}{r_0}\right)^6 \tag{6}$$

$$+\frac{1}{2}e\alpha U_{END}\left(\frac{r}{r_0}\right)^2 - e\alpha U_{END}\left(\frac{z}{r_0}\right)^2. \tag{7}$$

Laser and Sympathetic Cooling

Assume that barium ions have two electronic energy levels separated by $\Delta E = hf_r$, where h is Planck's constant and f_r is the resonance frequency of barium. When a photon of frequency f is incident onto the ion, it gets absorbed with some probability determined by the Lorentzian probability density function shown in FIG 4. As a result,

an electron jumps onto an excited state and sits there before decaying back to the ground state. The decay time follows the exponential distribution with the mean lifetime τ. While decaying, it emits a photon with a frequency following the same Lorentzian curve.

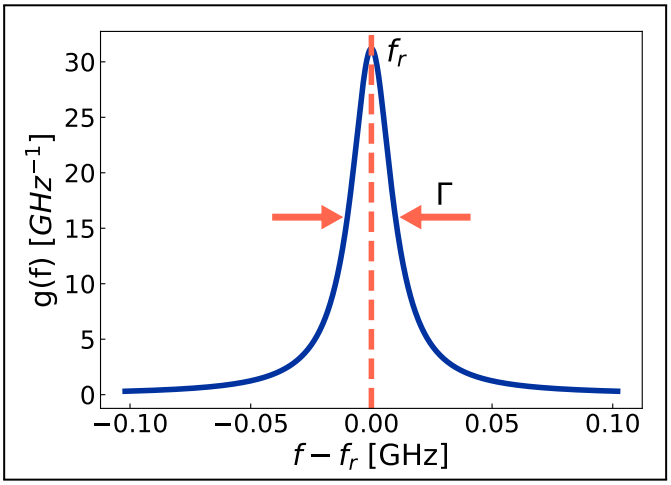

Figure 4. The Lorentzian distribution $g(f)$ which describes the probability of absorbing or emitting a photon with a frequency f.

If the lifetimes were infinite, the Lorentzian would have been a Dirac delta distribution, but due to the Heisenberg uncertainty principle it has a natural linewidth with a full width at half maximum of $\Gamma = \frac{1}{2\pi\tau} \approx 20.4$ MHz.

Now, assume that a barium ion moves with a velocity v projected onto the the laser axis in the opposite direction of the photon propagation. In the frame of the ion, the photon frequency f will be blueshifted to $f' = (1 + \frac{v}{c})f$. Therefore, if the laser frequency is tuned to a value just below the resonance frequency the ions will only absorb photons moving in the opposite direction of the ion which usually results in slowing down of the ion.

When an ion re-emits a photon, it receives a kick in an arbitrary direction resulting in a random walk in the momentum space. By studying the equilibrium of heating rates due to the emission recoiling and absorption cooling, one can obtain the lowest achievable energy using standard laser cooling called the Doppler limit[18]. Evaluating the Doppler limit formula for the Ba^+ ions yields $T_{Doppler} = \frac{\hbar\Gamma}{2k_B} \approx 0.5$ mK, where k_B is the Boltzmann constant. Such temperatures are reachable only if the micromotion vanishes and the collisions with nearby particles do not produce heating.

Although BaH^+ ions don't interact with the laser directly, they may get sympathetically cooled[8] by interacting with the Ba^+ ions via Coulomb interactions, as we will discuss in the next sections.

Methods

Before running a molecular dynamics simulation†, we needed to pick the trapping parameters. First, we picked the quadrupole stability parameters a and q. To achieve this, we generated stability diagrams using Floquet theory[19] and a COMSOL Multiphysics simulation (see FIG 5). The COMSOL stability diagram was obtained by releasing a particle with a radial velocity of 100 m/s from the centre of the trap and observing if it escaped the trap during a 10 μs simulation. Initially, the geometric parameter α was set to -1. Once the stability diagram was obtained, the value of α was found to be -0.024 by stretching the COMSOL-simulated diagram along the a-axis until it matched the Floquet diagram.

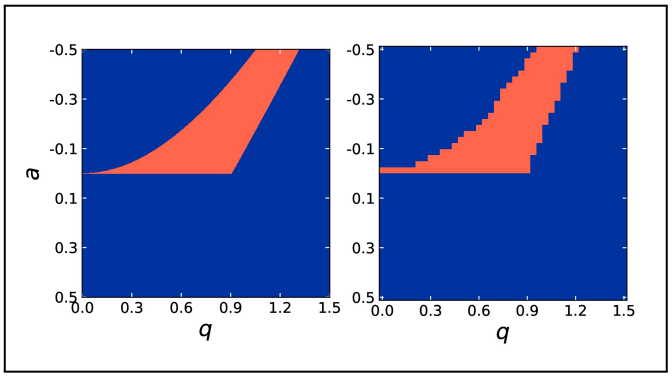

Figure 5. A Floquet stability diagram (left) and a COMSOL stability diagram (right). The (a,q) parameters in the orange region generate a bounded ion trajectory. Note that $a < 0$ to enable axial trapping.

For the quadrupole, we picked the voltage amplitudes $U_{END} = 8$ V and $V_{RF} = 160$ V with the frequency $f = 500$ kHz satisfying the stability points $(a,q) = (-0.001, 0.4)$. Note that the parameter a was chosen such that $-a << q^2$ to avoid radial defocussing effects.

For the octupole, we tried to pick as large V_{RF} as possible and as small U_{END} as possible to produce flatter trapping radial potential while maintaining stability. We ended up choosing $V_{RF} = 40$ V and $U_{END} = 1$ V with the frequency $f = 100$ kHz. To verify that these parameters produce a trapping potential with bounded ion trajectories, we performed a COMSOL simulations where we released a $2 \times 2 \times 2$ mm grid of 27 uniformly distributed ions with isotropic velocities 10 m/s from the centre of the trap and observed that all of the ions remained trapped during a 100 μs run.

To determine the octupole geometric parameter $\alpha = -0.039$, we studied the Z-amplitudes of charged particles

†The Python codes and COMSOL files can be found on GitHub: `https://github.com/NikitaPoljakov/CERN_Summer`

for a range of velocities in a COMSOL simulation. More specifically, the Z-amplitudes were fitted with a quadratic function Az^2, as predicted by the equation 7, which yields $\alpha = -\frac{Ar_0^2}{eU_{END}}$. The resulting radial potential is illustrated in FIG 3.

Once all the necessary parameters were obtained, we wrote a molecular dynamics simulation where the ions were evolved using the Euler method and interacted via Coulomb forces. The timestep of the Euler method was equal to that of the excited state lifetime $\tau = 7.8$ ns.

For both trap configurations, we used the RF equations for the X and Y motion to include the micromotion, and a pseudopotential approximation for the Z motion.

At the start of the simulation, the velocities of the ions were isotropic, as illustrated in FIG 6, and following a Maxwell-Boltzmann distribution at 1 K as seen in FIG 7. Both directions and speeds were selected using the accept-reject algorithm. The initial positions of 1000 ions were uniformly distributed over a cylinder for the quadrupole and a ring for the octupole as depicted in the FIG 8. The dimensions of these shapes were chosen such that they were not too big to avoid particles accelerating due to external electric fields, nor were they too small to avoid a Coulomb explosion where particles gain a significant energy from repulsion due to particle interactions.

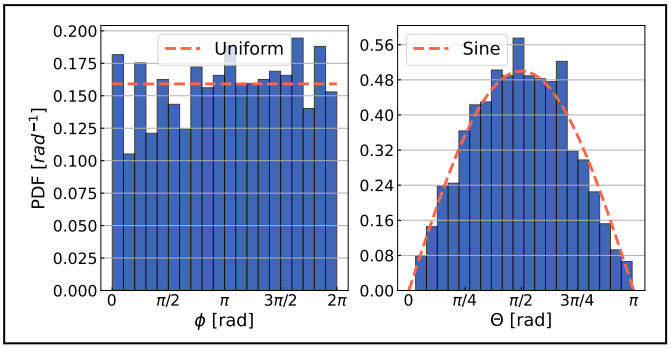

Figure 6. Initial azimuthal and polar velocity directions of 1000 particles. The former follows a uniform distribution and the latter follows a sine distribution such that the directions are uniformly distributed over a unit sphere.

As the simulation was set running, at each timestep, the excited ions re-emitted their photons and the ground-state ions could absorb photons which was decided by the accept-reject algorithm following the Lorentzian probability. We used six lasers in total, one counterpropagating pair for each of the X, Y, Z trap axes. The order of lasers used for the accept-reject algorithm was shuffled at random.

Note that we assume sufficiently wide laser beams such that particles at any position in the trap could interact with the laser. For the quadrupole trap, this would yield the beam width radii of $(r_x, r_y, r_z) = (0.1, 0.1, 2)$ [mm], and for the octupole, the beams would be $(r_x, r_y, r_z) = (0.8, 0.8, 2)$ [mm] wide.

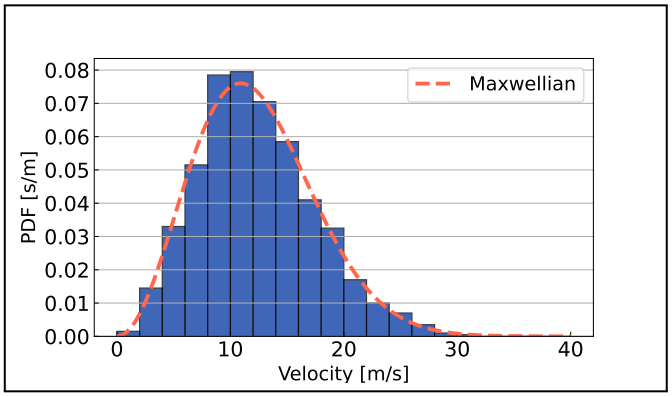

Figure 7. Initial speed distribution of 1000 ions at 1 K following a Maxwell-Boltzmann distribution.

To cool down ions at all speeds, the frequency of the laser was swept linearly from the minimal to the maximal value with a rate of order $\sim$ GHz/s, such that the cooling started with the hotter particles. The starting frequency was chosen such that it matched the Doppler-shifted resonance frequency of the Lorentzian of particles with the velocity projection onto the laser axis equal to the mean of the initial speed distribution. The final frequency was chosen such that the the upper half width at the half maximum of the Lorentzian curve corresponded to the frequency of the photons interacting with the particles at the recoil limit[18] $\nu_{recoil} = \frac{hf_r}{2mc}$ below which laser interactions can only cause heating. After the frequency sweep, the lasers were turned off for 0.1 ms to be able to study the final speed distributions without the laser interactions.

Results and Discussion

We show that it is possible to trap and cool 1000 ions, with an initial temperature of 1 K and laser cooling for 3 ms. The ions form structures shown in FIG 9.

By taking a radial cross-section of the quadrupole ion ensemble, as illustrated in FIG 10, we find that there is a clear boundary and internal structure indicating that the ions are in a crystal state. Although the octupole ion ring has a clear outermost boundary, it does not have an innermost one. This might be because the radial potential is steeper at the outermost part of the ring. Furthermore, FIG 11 does not indicate any internal structure and hence the octupole ions are in a liquid-gas state.

In FIG 10, we see that for the quadrupole case the

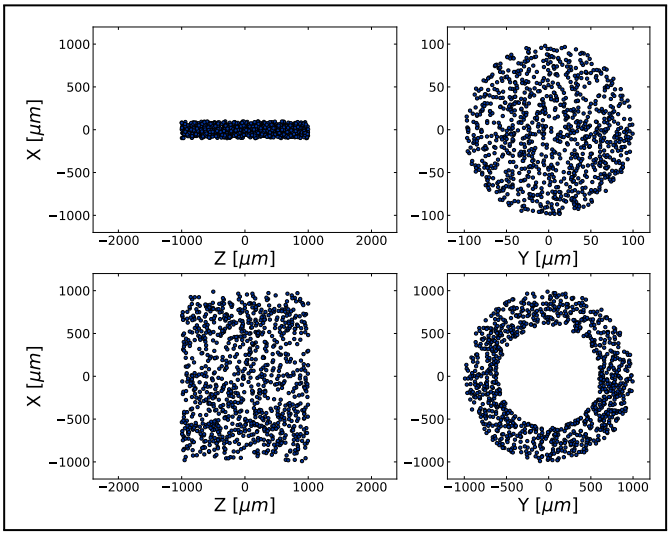

Figure 8. Initial positions of 1000 ions for the quadrupole (top) and an octupole (bottom) in the XZ (left) and XY (right) planes. For the quadrupole, the ions are uniformly distributed over a cylinder of radius 0.1 mm and height of 2 mm. For the octupole, the ions are uniformly distributed over a ring of radius 0.8 mm, radial thickness 0.4 mm and axial length 2 mm.

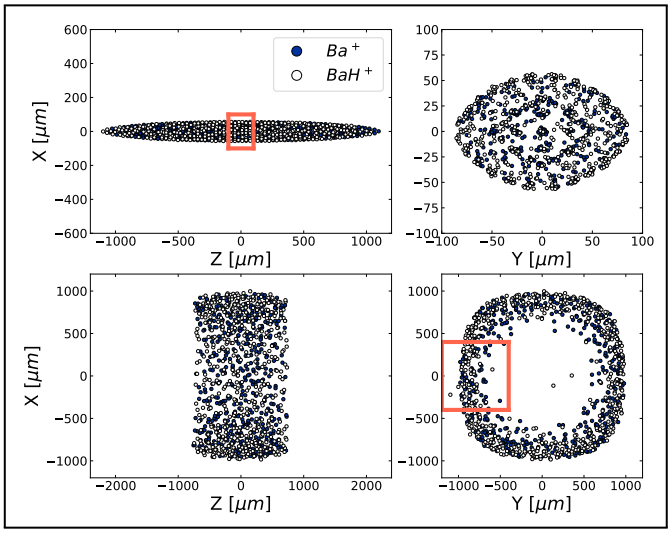

Figure 9. Final positions of 500 Ba^+ and 500 BaH^+ ions in a quadrupole (top) and octupole (bottom) potential. The regions marked with orange boundaries are shown in FIG 10 and 11.

ions group into Z-layers with spacing ~ 20 μm. The lighter Ba^+ ions are slightly closer to the axis than the heavier BaH^+ ions. As we zoom into the octupole ion ring in FIG 11, we don't see the separation of the ion species.

To quantify how hot the ions are, we have accumulated the ion velocities during the last secular period of the simulation (FIG 12). For the quadrupole, we get a speed cut-off at ~ 45 m/s and for the octupole the cut-off is at ~ 32 m/s. Note that the ions re not expected to follow the Maxwell-Boltzmann distribution because the presence of the trapping potential and micromotion cause the ions to deviate from the ideal gas approximation.

In FIG 13, we show the immediate temperatures of the hydrogen atoms if we photodissociated all BaH^+ ions at once. We have assumed that the energy carried by dissociating photons is equal to the bonding energy between Ba^+ and H and hence the daughter hydrogen atom moves with the same speed as its parent BaH^+ ion. We then converted the BaH^+ velocity distributions into temperature distributions using $\frac{3}{2}k_BT = \frac{1}{2}m_H v^2_{BaH}$, where we have assumed the equipartition theorem. Note that this assumption is more accurate for the lower temperature region of the hydrogen atoms because these hydrogen atoms are products of the near-axis BaH^+ ions where the micromotion vanishes and potential is flat.

For the quadrupole, approximately 38%, 13%, 5% of hydrogen atoms reach temperatures below 10, 1, 0.1 mK, respectively. The average hydrogen temperature is 24 mK. For the octupole, approximately 54%, 15%, 3% of hydrogen atoms reach temperatures below 10, 1, 0.1 mK, respectively. The average hydrogen temperature is 11 mK. Therefore, although there are more ultracold hydrogen atoms in the quadrupole trap, the octupole allows to reach a lower average temperature. This might be due to a flatter potential minimum where micromotion is less significant than in the quadrupole case.

A typical minimum B-filed Ioffe-Pritchard trap used for trapping antihydrogen in ALPHA is ~ 0.5 K meaning that all of the hydrogen produced in our simulations can foreseeably be trapped for precision measurements in the same ALPHA apparatus where antihydrogen precision measurements take place[20].

Notice that in a quadrupole trap the BaH^+ ions get hotter with radial distance as seen in 14. This temperature gradient can be used to achieve even lower hydrogen temperatures. Instead of photodissociating BaH^+ ions over the whole ensemble, we can do this only with the ions close to the axis. In particular, by shining a photodissociating laser beam of radius 5 μm along the trap z-axis, we would obtain ~ 40 μK hydrogen. However, such approach would produce less hydrogen unless it is possible to cool down new BaH^+ ions from the outermost layers of the ensemble and replace the dissociated Ba^+ ions near the axis.

In future investigations, finite cooling laser beam widths could be included in the simulation. Another idea is to study how the 1 K ions evolve in the same traps without the laser. Furthermore, the behaviour with

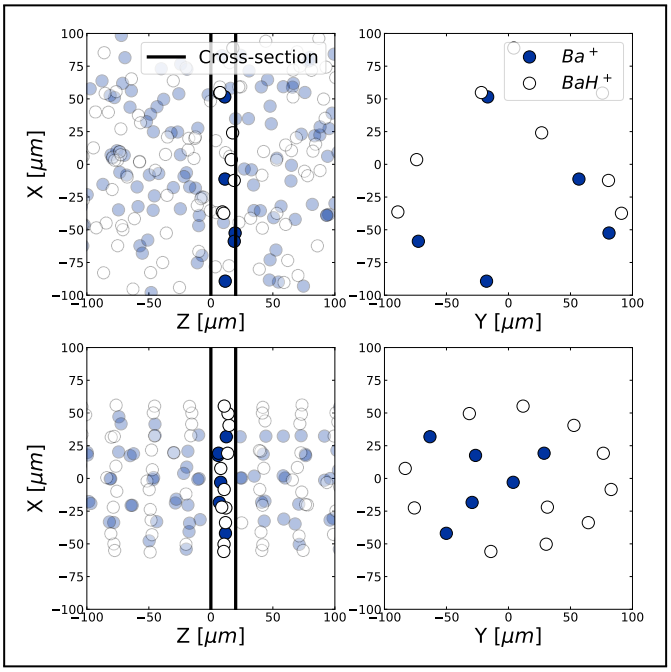

Figure 10. Cross-sections of the initial (top) and final (bottom) positions of ions in the $z \in [0\mu\text{m}, 20\mu\text{m}]$ axial interval in the quadrupole simulation.

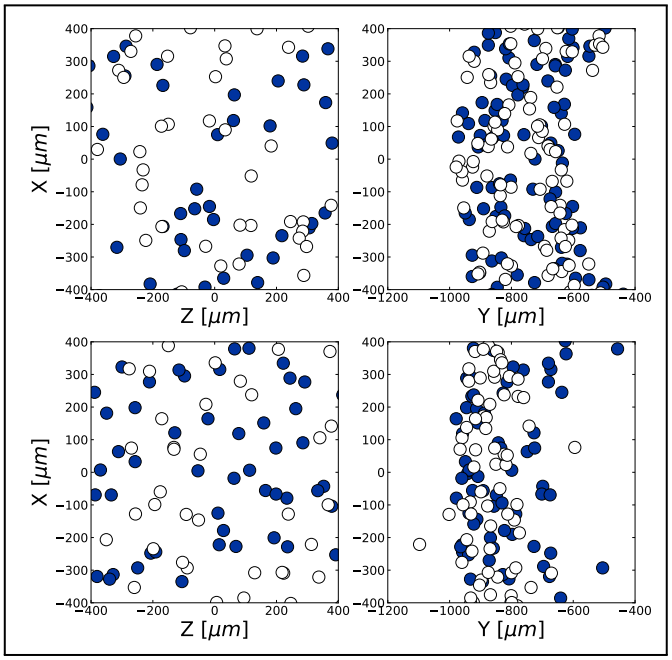

Figure 11. Zoomed-in plots of the initial (top) and final (bottom) ion positions in the octupole simulation.

higher initial temperatures could be studied and the temperature evolution of ions investigated. To make the simulation more realistic, trap imperfections, such as the residual gas and rod asymmetries could be incorporated.

Alongside laser and sympathetic cooling, other cooling methods can be studied. For example, adiabatic cooling[21] can be used to bring ion ensembles to even lower temperatures by lowering the pseudopotential and making ions perform work on the potential walls. However, this method will cause ions to occupy larger space and fewer ions will have negligible micromotion.

Conclusion

Trapping and cooling of $^{138}Ba^+$ and $^{139}BaH^+$ ions has been simulated in linear RF quadrupole and octupole traps. We considered two specific quadrupole and octupole configurations and showed that after photodissociation of BaH^+ ions, hydrogen reaches lower temperatures in the octupole case with the mean value of 11 mK than in the quadrupole case with the mean value of 24 mK.

Acknowledgments

I am very grateful to my supervisor Dr. Muhammed Sameed and the author of the project idea Dr. Steven Armstrong Jones for fruitful meetings and stimulating discussions. Thank you for motivating me during this project and encouraging to continue the path of a researcher.

I would also like to thank the CERN Summer Student Program organizers and lecturers for this rewarding summer experience.

References

[1] The ALPHA Collaboration and A. E. Charman. Description and first application of a new technique to measure the gravitational mass of antihydrogen. *Nature Communications*, 2013.

[2] A. I. et al Zhmoginov. Nonlinear dynamics of antihydrogen in magnetostatic traps: implications for gravitational measurements. *IOP*, 30, 2013.

[3] The ALPHA Collaboration. Observation of the 1S–2P Lyman-α transition in antihydrogen. *Nature*, 561:211–218.

[4] The ALPHA Collaboration. Observation of the 1S–2S transition in trapped antihydrogen. *Nature*, 541:506–512, 2017.

[5] S. A. Jones. Observation of the 1S-2S transition in trapped antihydrogen. *PhD thesis*, 578, 2017.

[6] The ALPHA Collaboration. Investigation of the fine structure of antihydrogen. *Nature*, 578:375–384, 2020.

[7] W. A. et al Bertsche. Physics with antihydrogen. *IOP*, 48:375–384, 2015.

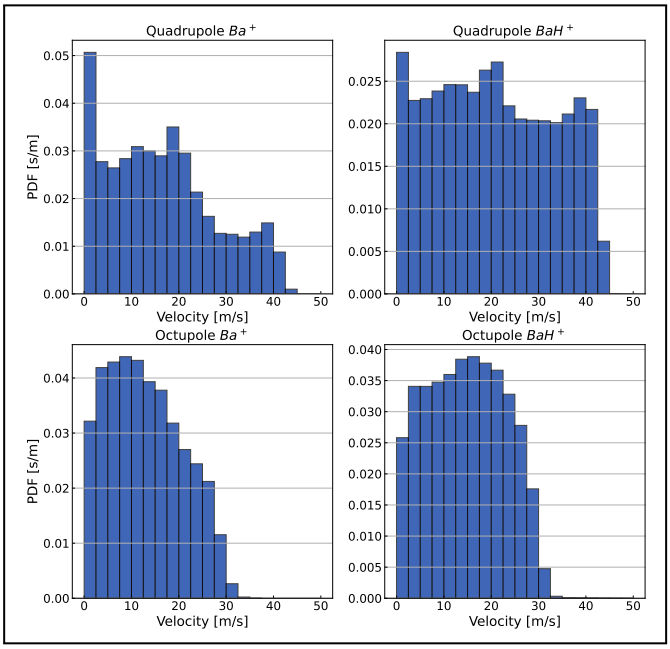

Figure 12. Speed distributions accumulated over the final secular period of the simulation for both the quadrupole and octupole simulations.

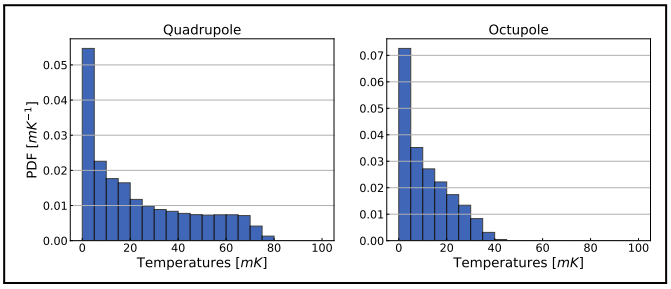

Figure 13. Hydrogen temperature distribution after photodissociating all BaH^+ ions at once.

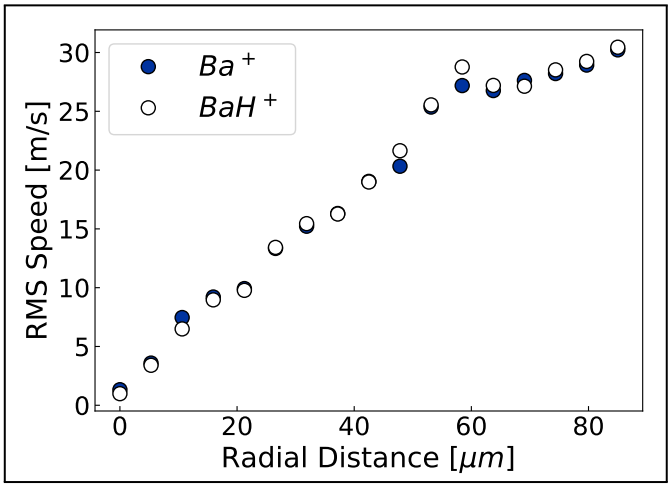

Figure 14. RMS speeds of ion ensembles belonging to 5 μm thick radial layers in the equilibrium ellipsoidal shape produced in the quadrupole simulation. As expected, the micromotion increases with the radial distance linearly. BaH^+ ions in the first shell have a RMS speed of ~ 1.0 m/s.

[8] E. R. Hudson. Sympathetic cooling of molecular ions with ultracold atoms. *EPJ Techniques and Instrumentation*, 2016.

[9] S. A. Jones. An ion trap source of ultracold atomic hydrogen via photodissociation of the bah+ molecular ion (manuscript in preparation).

[10] S. Schiller and C. Laemmerzahl. Molecular dynamics simulation of sympathetic crystallization of molecular ions. 2018.

[11] M. Marciante, C. Champenois, A. Calisti, J. Pedregosa-Gutierrez, and M. Knoop. Ion dynamics in a linear radio-frequency trap with a single cooling laser. 2014.

[12] M. Drewsen and A. Brøner. Harmonic linear paul trap: Stability diagram and effective potentials. *Physical Review*, 62, 2000.

[13] W. Paul. Electromagnetic traps for charged and neutral particles. *Reviews of Modern Physics*, 62(3), 1990.

[14] P. H. Dawson. *Quadrupole Mass Spectrometry and its Applications*. Elsevier, 1976.

[15] K. Okada, K. Yasuda, and T. Takayanagi. Crystallization of Ca+ ions in a linear rf octupole ion trap. *Physical Review*, 75, 2007.

[16] D. Gerlich. Ion-neutral collisions in a 22-pole trap at very low energies. *Physica Scripta*, T59:256–263, 1995.

[17] G. Z. et al Wilcox. Improved ion extraction from a linear octopole ion trap: SIMION analysis and experimental demonstration. *American Society for Mass Spectrometry*, 13:1304–1312, 2002.

[18] V. S. Letokhov. Quantum and semiclassical optics: Journal of the european optical society. *Reviews of Modern Physics*, 1995.

[19] I. Kovacic, R. Rand, and S. M. Sah. Mathieu's equation and its generalizations: Overview of stability charts and their features. *Applied Mechanics Reviews*, 70, 2018.

[20] The ALPHA Collaboration. The ALPHA antihydrogen trapping apparatus. *Elsevier*, 735:319–340, 2013.

[21] G. Z. et al Li. Adiabatic cooling of antiprotons in a Penning trap. *Hyperfine Interactions*, 76:281–284, 1993.